Pair creation enhancement due to combined external fields

M. Jiang,[1] W. Su,[2] Z. Q. Lv,[2] X. Lu,[1] Y. J. Li,[2] R. Grobe,[3,4] and Q. Su[1,4]

[1]*Beijing National Laboratory for Condensed Matter Physics, Institute of Physics, Chinese Academy of Sciences, Beijing 100190, China*

[2]*China University of Mining and Technology, College of Sciences, Beijing 100083, China*

[3]*Max-Planck-Institut für Kernphysik, Saupfercheckweg 1, D-69117 Heidelberg, Germany*

[4]*Intense Laser Physics Theory Unit and Department of Physics, Illinois State University, Normal, Illinois 61790-4560, USA*

(Received 22 December 2011; published 7 March 2012)

We study the creation of electron-positron pairs from the vacuum induced by a combination of a static electric field and an alternating field. We find that the overall pair production can be increased by two orders of magnitude compared to the yields associated with each field individually. We examine the interesting case where both fields are spatially localized, permitting us to examine the time evolution of the spatial density for the created particle pairs. We find that there are a variety of competing mechanisms that contribute to the total yield.

DOI: 10.1103/PhysRevA.85.033408 PACS number(s): 34.50.Rk, 03.65.−w

I. INTRODUCTION

The creation of electron-positron pairs from a constant electric force field was first calculated by Sauter [1] and Schwinger [2], which has brought much attention to this fascinating research area. Since then many more studies have followed and extended the pair creation by a constant field to more general space- and time-dependent forces. There are a few different mechanisms under which an intense field can "break down" the vacuum and create particles. In the first one, a threshold is required for the static field ($E_c = 1.32 \times 10^{16}$ V/cm) and a permanent flow of particles can be generated only if the field is supercritical. The second mechanism is due to the time dependence of the field that will induce quantum transitions where the photon energy plays a key role [3–12]. A third mechanism shows that pair creation can also be realized due to quantum mechanical tunneling between two spatially nonoverlapping force fields [13]. It can be observed if two static and subcritical electric fields are separated by less than the quantum mechanical tunneling length.

Unfortunately experimental attempts to observe this intriguing phenomenon of the direct conversion from light to particles have been unsuccessful. Beginning in the 1980s it was attempted to create a supercritical field via two overlapping Coulomb fields associated with two colliding heavy ions [14–16]. Some positrons were measured but it is believed today that their main production mechanism was not necessarily caused by the Coulombic field itself, but by nuclear transitions, which are unavoidable in highly relativistic collisions.

In another pioneering experiment at SLAC an electron beam was collided with an intense laser pulse and generated positrons were detected [17,18]. In this process the interaction of the high energetic electrons and the laser beam was essential to the generation of electron-positron pairs. While this experiment was operated essentially in the perturbation domain, it did reveal the onset of nonperturbative signatures [19,20]. It would be interesting to see how the pair creation will be affected if one could collide γ photons directly with an intense laser beam [21].

In this work we examine the time dependence of the pair-creation probability for a two-field configuration of an alternating field and a static field. In contrast to some previous works, we investigate the case where both fields have a finite spatial extend. While this assumption makes the theoretical approach much more complicated, it permits us to study also the spatial evolution of the created particle pairs. We find that the increased parameter space of externally varying field strength provides a rather rich and unexpected dynamics, characteristic of decreasing particle yields with increasing field strengths and regions in which an additional field can actually suppress the pair-creation process. We examine the high-frequency regime where the mechanisms discussed above can compete and discuss the optimal physical parameters to maximize the amount of pair creation.

We compute the time dependence of the pair-creation probability for such a two-field configuration from the quantum field operator. The operator's space and time dependence is constructed numerically from the relativistic quantum mechanical solutions to the time-dependent Dirac equation [22–25]. This computational approach to quantum field theory has been introduced recently to study the pair-creation process with full space-time resolution. For a recent review see Ref. [26]. It can provide an alternative approach to the traditional S-matrix approach, which is based on the in and out states only and therefore cannot visualize the processes inside the interaction zone. In addition to visualizing the details of the pair-creation dynamics, direct time-dependent quantum field theoretical solutions to the Dirac equation have also contributed to the resolution of various conceptual problems related to the negative energy states such as the Zitterbewegung [27], the relativistic localization problem [27], as well as the Klein paradox [28–31].

This paper is organized as follows. In Sec. II we introduce our model system characterized by a subcritical time-dependent field and a supercritical static field, and present results of the created particle numbers for various frequencies in Sec. III. In Sec. IV we study the spatial distribution of created particles and their developments with time. In Sec. V we discuss the energy spectra of the created electrons and their scaling with respect to the field strength. In Sec. VI we provide a summary, determine if the yield is mostly due to single or multiple pairs, and outline further research directions.

II. QUANTUM FIELD THEORETICAL SIMULATIONS

In order to describe the electron-positron creation process, the relativistic quantum mechanical (Dirac) equation for a

single-particle wave function is not sufficient as it assumes the existence of a particle from the beginning and the unitary time evolution would make it impossible to describe processes for which the number of particles can change. To describe creation and annihilation processes we need quantum field theory, where the evolution of operators is obtained from the Heisenberg equation of motion using the quantum field theoretical Hamiltonian. However, as we are neglecting interfermionic interactions, it turns out that the evolution of the quantum field operator $\hat{\Psi}(t)$ is also described by the Dirac equation (in atomic units from now on)

$$i\partial\hat{\Psi}(z,t)/\partial t = [c\alpha_z p_z + \beta c^2 + V(z,t)]\hat{\Psi}(z,t). \quad (2.1)$$

Here $V(z,t)$ denotes the scalar potential associated with the external force acting along the z direction, while α_z denotes the z component of the Dirac matrix, β is the diagonal Dirac matrix, and c is the speed of light. We can expand $\hat{\Psi}(z,t)$ in terms of creation and annihilation operators and the force-free positive and negative energy eigenstates $|p\rangle$ and $|n\rangle$, and their spatial representation $u_p(z)$ and $v_n(z)$ according to

$$\begin{aligned}\hat{\Psi}(z,t) &= \sum_p \hat{b}_p(t)u_p(z) + \sum_n \hat{d}_n^\dagger(t)v_n(z) \\ &= \sum_p \hat{b}_p u_p(z,t) + \sum_n \hat{d}_n^\dagger v_n(z,t). \quad (2.2)\end{aligned}$$

The electronic portion of the field operator associated with positive energy can be defined as

$$\hat{\Psi}^{(p)}(z,t) \equiv \sum_p \hat{b}_p(t)u_p(z), \quad (2.3)$$

where $u_p(z)$ is the eigenvector of force-free Hamiltonian with positive energy. The time-dependent number of created particle pairs can be computed from the vacuum (initial) state through

$$N(t) \equiv \sum_p \langle\langle \text{vac}||\hat{b}_p^\dagger(t)\hat{b}_p(t)||\text{vac}\rangle\rangle \quad (2.4)$$

and created particle spatial density is defined here as

$$\rho(z,t) \equiv \langle\langle \text{vac}||\hat{\Psi}^{\dagger(p)}(z,t)\,\hat{\Psi}^{(p)}(z,t)||\text{vac}\rangle\rangle. \quad (2.5)$$

These two quantities are related with each other via $N(t) = \int dz\ \rho(z,t)$. Using the two equivalent expressions for the time evolution of $\hat{\Psi}(z,t)$ in Eq. (2.2), we can solve for $\hat{b}_p(t)$ required in Eq. (2.4). Making use of the initial state property $\hat{b}_p||\text{vac}\rangle\rangle = 0$ and after some operator algebra we obtain for the total number of created pairs

$$N(t) = \sum_{p,n} |U_{p,n}(t)|^2 \quad (2.6)$$

and for the spatial density

$$\rho(z,t) = \sum_n \left| \sum_p U_{p,n}(t)\, u_p(z) \right|^2. \quad (2.7)$$

Here the matrix elements $U_{p,n} \equiv \langle p|n(t)\rangle$ can be computed by evolving the Dirac wave equation starting from negative energy states $|n\rangle$. The evolved state $|n(t)\rangle$ is projected onto all positive energy force free states $|p\rangle$. The single-particle Dirac equation from state $|n\rangle$ is solved numerically using a split-operator technique [22–25], where the states are discretized on a numerical grid of length L with N_z spatial grid points. In this method the time-evolution operator $\exp(-iht)$ is decomposed into N_t consecutive actions, each subinterval operators can be approximated by $\exp(-iht) \approx \exp(-iV\Delta t/2)\ \exp(-ih_0\Delta t)\ \exp(-iV\Delta t/2)$, where h_0 denotes the force-free Hamiltonian. The action of $\exp(-iV\Delta t/2)$ can be performed conveniently in the discretized coordinate space with N_z grid points. By using the Fourier transformation between the spatial and momentum representations, we can compute the action of the corresponding propagators via simple multiplications in the relevant space.

III. THE TIME-DEPENDENT PAIR-CREATION PROBABILITY

Here we use the one-dimensional simulation introduced in Sec. II and characterize the field with a scalar potential $V(z,t)$ along the z direction. In our model, the first field of amplitude V_1 is subcritical and varies sinusoidally with time, while the second field V_2 is supercritical and independent of time, $V(z,t) = V_1\ S(z)\ \sin(\omega t) + V_2\ S(z)$. Here the function $S(z)$ represents the Sauter potential, $S(z) \equiv \{1 + \tanh[(z - z_0)/W]\}/2$, modeling an electric field that is concentrated around z_0 with spatial width W [1]. This form of the potential $V(z,t)$ permits us to study the effect of a combination of a time-dependent field with a static external field for the interesting case where *both* fields are spatially localized. In this section we set the field strengths to $V_1 = 1.47c^2$ and $V_2 = 2.53c^2$ and vary the frequency between $\omega = 1.5c^2$ and $2.5c^2$.

As mentioned in the Introduction, there are two distinctly different mechanisms to create particle pairs from the vacuum. The first one is the traditional Schwinger mechanism which does not require any time dependence but simply a supercritical potential strength $V > 2c^2$. The second mechanism is exclusively associated with the time dependence of the external field, which for any amplitude or frequency can trigger a transition from states of the negative to the positive energy continuum [31]. In order to study the interplay between these two mechanisms, we present in Fig. 1 the time evolution of total pair-creation $N(t)$, defined in Eq. (2.4).

It turns out that the data for $N(t)$ for various field configurations are remarkably complicated and therefore require a rather detailed discussion.

A. The yield $N(t)$ associated with each field separately

To set the scale, let us first show the negligible impact on the pair-creation process due to the separate actions of the oscillating and static fields alone. The three dashed curves correspond to the pair creation due to the static field only ($V_1 = 0$). Even though their amplitudes $V_2 = 1.06c^2$, $V_2 = 2.53c^2$, and especially $V_2 = 4c^2$ makes these potentials (at least from a technical point of view) supercritical leading to a slightly positive slope of the graph, the permanent creation of electrons is rather negligible on our short time scale $T = 2 \times 10^{-3}$ a.u. and leads to only $N(T) = 0.018$ for $V_2 = 2.53c^2$. Here the slow pair creation is also consistent with the relatively small magnitude for the corresponding external field which for our width $W = 6/c$ at its peak is $V_2/(2W) = 2.5c^2/(6/c) = 0.4c^3$.

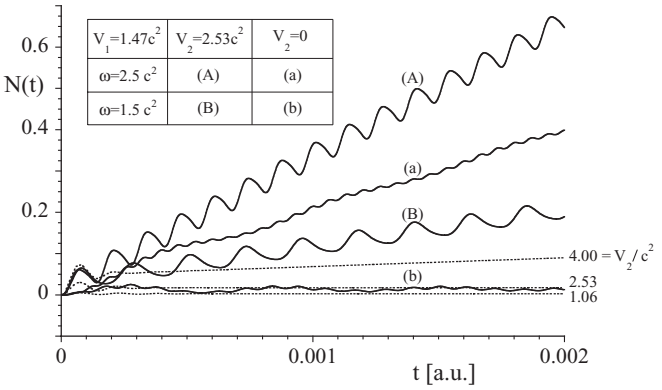

FIG. 1. Time evolution of the total number of pairs $N(t)$ for various field configurations. Graph (A): ($\omega = 2.5c^2$, $V_2 = 2.53c^2$). Graph (a): ($\omega = 2.5c^2$, $V_2 = 0$). Graph (B) ($\omega = 1.5c^2$, $V_2 = 2.53c^2$). Graph (b) ($\omega = 1.5c^2$, $V_2 = 0$). The amplitude of the oscillating field is always $V_1 = 1.47c^2$, except for the three dashed lines, which correspond to the static fields only ($V_1 = 0$), where $V_2 = 1.06c^2$, $2.53c^2$, and $4c^2$ [$W = 3/c$, $L = 1.2$, $N_z = 512$].

This value is less than the Schwinger field E_c, which in atomic units amounts to c^3.

Let us now analyze the two curves obtained for the case where the electrons are created by the oscillating field alone ($V_2 = 0$). The lowest solid curve, labeled with (b), at the bottom of Fig. 1 is for $V_1 = 1.47c^2$ and $\omega = 1.5c^2$. Here the curve is slightly oscillatory but the overall yield [$N(T) = 0.012$] is again almost negligible. A frequency only $\omega = 1.5c^2$ is essentially insufficient as its "photon" energy is not sufficiently large enough to bridge the energy gap of $2c^2$. To make a transition a two-photon transition is needed. For the current excitation, two-photon transition amplitude is much smaller than the one-photon transition.

The second solid curve labeled with (a) corresponds to pair creation where the amplitude is the same ($V_1 = 1.47c^2$) but the frequency is larger $\omega = 2.5c^2$. The total pair creation has been enhanced for this frequency as one photon is sufficient to enable the transition between negative and positive energy states. Such a transition, according to Eq. (2.6), is responsible for the increase in pair creation. For example, at time $T = 0.002$ total creation has reached about 0.4, a more than 20-fold enhancement compared to the two processes for ($V_1 = 1.47c^2$, $V_2 = 0$, $\omega = 1.5c^2$) and ($V_1 = 0$, $V_2 = 2.53c^2$).

In addition to the overall linear increase and the difference in pair-creation rate, both curves (a) and (b) oscillate in time with frequency 2ω. This response is rather generic for driven quantum systems, where the yield is typically related to the square of the external amplitude. A good example would be the time dependence of the photoionization probability, where during one oscillation period of the intensity assumes its maximum value twice.

B. The yield $N(t)$ associated with a combination of both fields

The combination of both fields ($V_1 = 1.47c^2$, $\omega = 1.5c^2$) and $V_2 = 2.53c^2$ leads to a significant enhancement of the pair-creation rate as indicated by the graph labeled (B), corresponding to an enhancement of the final number of particles by a factor of 10 [from $N(T) = 0.018$ to $N(T) = 0.18$]. In fact, it even exceeds the yield created by static field (upper dashed line) $N(T) = 0.09$, whose strength ($4c^2$) is identical to the maximum value the combination of both fields can take, $V_1 + V_2$.

The period of the superimposed oscillations matches the period of the time-dependent field $2\pi/\omega = 2.2 \times 10^{-4}$ a.u. It is rather interesting, that in contrast to the fast (2ω) oscillations for $V_2 = 0$, the yield $N(t)$ oscillates now only with half the frequency. When V_2 is gradually increased the frequency of oscillation switches from 2ω to ω. The effective field due to the combination of both fields changes the amount of its amplitude from its maximum value $V_{\max} \equiv V_2 + V_1$, to its minimum value $V_{\min} \equiv |V_2 - V_1|$. In other words, the field might be strong enough to trigger the pair creation only during first half of the period while during the second half the creation might be stopped. For the parameters presented in Fig. 1, during the peak time of the oscillatory field the total field is given by $V_{\max} = 4c^2$, whereas a half period later the negative amplitude leads to an instantaneous field of only $V_{\min} = 1.06c^2$. The sign of our potential is chosen such that an electron would be accelerated to the right. For even a larger value of V_2 those particles that are moving to the left after the creation would be forced by the static field to come back to the interaction region. As a result, some of the created particles could be annihilated again [31]. There could be also Pauli blocking [28,30] to reduce further creation and this would be responsible for pair creation to decrease during the second half of the period and producing the temporal variation that is characteristic of curve (B).

We might add a small caveat to our discussion. As the definition of the particle yield in Eq. (2.6) is based on force-free states, one has to be careful with the interpretation of $N(t)$ for those particles that are located inside the creation zone. However, an improved definition of the yield inside the supercritical zone is very difficult to define, as it is nontrivial and a presently unresolved conceptual challenge.

In addition to the change in frequency, there are some additional interesting details in the temporal behavior in Fig. 1. A closeup of these oscillations shows that they cannot be described by a simple sum of a linearly increasing function of time with a sine or cosine function, as one could expect. In fact, for a function of the type $\sim t + \sin \omega t$ the length of the graph from minimum to maximum is always longer than the length it takes to return back to the minimum value. The graph (B), however, shows an opposite behavior characteristic of a (steeper) rise and (more gradual) fall of the particle yield within each cycle.

For a better comparison, we have also shown the data (A) for the case where the frequency of the alternating field is sufficiently large to exceed the energy gap, $\omega = 2.5c^2$. While $N(t)$ grows still in an oscillatory fashion with the *full* period corresponding to $2\pi/\omega$, the asymmetry between the gradual rise and the steep fall within each cycle resembles that of a decaying system in which the transitions are due to the absorption of a photon with energy ω. As in this case, we have a more rapidly oscillating field, also the slope of the graph is larger than that of graph (B).

While similar to graph (A) the frequency of variation around the linear rise is ω, there is a visible difference between (B) and (A). The frequency used in (B) is too small to allow a single photon transition as in (A). Since the energy $\omega = 1.5c^2$

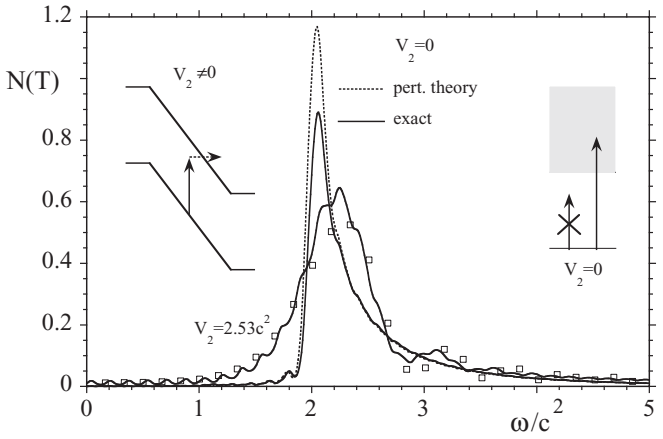

FIG. 2. Total number of created pairs $N(t)$ at final time $T = 0.002$ a.u. as a function of frequency ω for $W = 5/c$, $V_1 = 1.47c^2$ and $V_2 = 0$ (the narrower curve) or $V_2 = 2.53c^2$ (the wider curve). The dashed line is the prediction based on perturbation theory (see Appendix A), the squares are due to the two-level model (see Appendix B) [$L = 1.2$, $N_z = 512$].

alone is not sufficient for a single photon absorption for curve (B), the additional Schwinger tunneling is needed to make a final transition to the positive energy manifold. The reversal of the oscillating field V_1 changes only the effective field for the tunneling reflected in the asymmetric shape of the rising and trailing edges within each cycle for graph (B).

C. The final yield $N(T)$ as a function of the frequency of the field

From the above observations it is safe to say that a combination of V_1 and V_2 can enhance the pair creation relative to the separate application of each field one at a time. However, the drastic increase of the yield when the frequency ω was changed from $1.5c^2$ to $2.5c^2$ suggests a more systematic study. In order to examine how the pair creation depends on the frequency of the alternating field we choose time $T = 0.002$ and display in Fig. 2 the final created particle number $N(T)$ as a function of frequency ω between 0 and $5c^2$.

1. *The final yield N(T) due to the oscillating field* ($V_2 = 0$)

To analyze the Schwinger tunneling and temporally induced process separately, we first omit the static field ($V_2 = 0$). The small superimposed oscillations in the graph have a period of $0.17c^2$, which is roughly half of $2\pi/T = 0.33c^2$. In other words, these small oscillations are due to the finite interaction time T and would disappear for $T \to \infty$.

We observe a rapid rise of $N(T)$ when the frequency exceeds the energy gap $2c^2$, while the pair production stays essentially zero for $\omega < 2c^2$, consistent with our earlier observation. It is interesting that there is small amount pair creation for ω between c^2 and $2c^2$, which can be explained in terms of a two-photon process making a transition between negative and positive energy states. However, the magnitude for this process is much smaller than that of the single-photon process as suggested by the inset on the right side. In fact, for even higher resolution calculations we found an even smaller contribution when $\omega = 2c^2/3$, permitting the onset of three-photon excitations. The yield of these two- and three-photon processes can be increased if the width W is decreased leading to an effectively larger electric force. All of these features are very similar to the multiphoton photoelectric effect of atomic ionization. The single and multiphoton-like transitions resulting in pair creation follows a power law of the intensity, where in our case $V_1{}^2$ serves as the intensity for the excitation, while the energy of the final states is basically determined by the frequency.

For larger frequencies, $N(T)$ decreases until it almost vanishes around $\omega > 4c^2$. This high-frequency decrease can be understood from an energetic as well as space-time resolved perspective. Larger frequencies excite high-energetic electrons but as the relevant coupling matrix element $\langle p|V|n\rangle$ decreases with increasing final momentum p, the yield has to decrease as well (see Appendix A). Equivalently, as the maximum speed the particles can gain has an upper limit, for large ω the electron-positrons do not have sufficient time to split and are unable to escape from the interaction region before a half cycle later the force direction is reversed and the created particles are annihilated again, as shown in Refs. [12,31].

For comparison, we show by the dashed line the corresponding yield obtained from a time-dependent perturbation theory calculation, whose details we present in Appendix A. Except for the threshold region around $\omega = 2c^2$, all details including the finite-duration induced oscillations are reproduced. In fact, even the kinks at $\omega = c^2$ and $\omega = 2c^2/3$ are reproduced if we extend the perturbation to include second- and third-order effects.

2. *The final yield N(T) due to the combination of the oscillating and static fields*

If we repeat the set of simulations with an additional static potential present with strength $V_2 = 2.53c^2$, we obtain the other solid-line graph shown in the figure. Here the small oscillations are again a finite-pulse effect as discussed above. As the static field is now present in addition to the oscillating field one could expect a larger particle yield for any frequency.

Rather surprisingly, this is not always the case. In fact, for the two small frequency windows $1.95c^2 < \omega < 2.15c^2$ and $2.68c^2 < \omega < 2.95c^2$, the presence of the static potential seems to have an *inhibiting* effect on the creation rate. The physical mechanism leading to these two windows of suppression will be discussed below.

By adding the static field, there are several mechanisms that contribute to the overall distribution compared to the single field case. First of all, for $\omega < 2c^2$ the previously "forbidden" region now becomes allowed, therefore enhancing the pair creation significantly. For frequencies around $\omega = 1.5c^2$, for example, it is enhanced by a factor of more than 10. Next, the maximum of pair production has been reduced from the amount for $V_2 = 0$ by a factor of 2 to about $N(T) = 0.6$ and the frequency for maximum pair creation has been shifted to larger frequency of about $\omega = 2.3c^2$. Finally for $\omega > 2c^2$ the amount of pair creation approaches the yield for $V_2 = 0$.

As we have argued above, for $V_2 = 0$ and $\omega < 2c^2$ the pair creation cannot be due to a single-photon process while the magnitude for the two-photon process is small. The reason

for the remarkably large amount of pair creation for $V_2 \neq 0$ between $\omega = 1.45c^2$ and $\omega = 2c^2$ could be explained in terms of a combination of a single-photon transition and the Schwinger tunneling as suggested by the sketch of the left inset of the figure [32–34]. It shows two potentials that are displaced vertically by the energy gap $2c^2$. A single photon is not possible to bridge the energy alone as indicted by the vertical arrow in the figure. If we allow a subsequent tunneling, which we assume to occur if the tunneling length is less than the Compton length $\lambda_c = 1/c$, the estimated minimum value of the frequency turns out to be about $\omega = 2c^2 - V_2\lambda_c/W_2 = 1.49c^2$. This frequency corresponds roughly to the frequency at which the static field can permit the pair creation.

Between $\omega = 2.5c^2$ and $3.5c^2$ there is an interesting additional oscillation of period $\Delta\omega = 0.51c^2$ with two minima around $\omega \approx 2.8c^2$ and $\omega \approx 3.4c^2$. In this frequency range the pair creation is due to single-photon transition. In the absence of any static potential, the created particles would escape with equal likelihood to the right and left of the potential. Due the static field, however, the right-moving particles are accelerated out of the interaction region while the left-moving particles are decelerated. Left going particles can therefore return to the interaction region and interfere with the production process. While interfermionic interactions are excluded in our approach, the Pauli exclusion principle is still applicable and reduces the production rate, if electrons occupy the relevant regions in space. This Pauli-blocking inhibition mechanism associated with returning particles is rather sensitive to the choice of the frequency as well as the birth velocity distribution. It could possibly explain the nonmonotonic behavior of the yield in this region between $\omega = 2.5c^2$ and $3.5c^2$. A numerical fit for large ω indicates the power-law dependence with effective powers of about 3 (for $V_2 = 0$) and 4 (for $V_2 = 2.53c^2$).

Regular time-dependent perturbation theory successfully explains the dynamics for $V_2 = 0$, but it fails for $V_2 \neq 0$. In order to model the combined action of both fields, we used the two-level approximation as discussed in Appendix B. This approximation can be used if the spatial width W is much larger than the Compton wavelength. It is actually exact if we were to replace the spatially localized electric fields associated with the Sauter potential $S(z)$ with a spatially constant (and therefore infinitely extended) electric field, associated with $S(z) = z/(2W)$. In this special case, an initial state of the negative energy continuum is coupled only to a single state with positive energy, like a two-level system [4,12,35,36]. In this simplifying model most of the essential features such as energy shifts, the multiphoton transitions, and the Schwinger tunneling are included. The predicted yield due to such an approximation is shown in Fig. 2 by the open squares. It is remarkable how this simple model is able to reproduce most the features of the numerical simulation while regular perturbation fails. Except for the threshold region close to $\omega = 2c^2$, where the dynamics is most complex and hard to model, the match is excellent. The match becomes less ideal when the external field width is on the order of Compton wavelength as strong field variation can no longer be approximated by a constant field. In addition to the two-level model described here, in the below-threshold region, when $\omega < 2c^2$, our result agrees also (not shown in Fig. 2) with the expression obtained for high-frequency field catalyzed Schwinger pair production rate using the worldline instanton method [33].

IV. SPATIAL DENSITY AND EFFECT OF POTENTIAL HEIGHT

In this section we accompany the findings of the prior section and study the spatial distribution of the created electrons. We also examine the surprising role the height of the static potential V_2 plays in enhancing but also inhibiting the pair creation. In Fig. 3 we show four temporal snapshots of the electron's spatial density $\rho(z,t)$ for the two frequencies $\omega = 1.5c^2$ [Fig. 3(a)] and $\omega = 2.5c^2$ [Fig. 3(b)] studied in the previous section. The corresponding distribution of the created positrons can be obtained by reflecting the electronic distribution around the center of the fields z_0, which we chose here as -0.3 a.u.

Figure 3 suggests that the electrons are pulled out from the center part by the static field and the edge of the distribution moves with a constant velocity of $v_c = 125$ a.u. or about 91% the speed of light. This corresponds to the linear growth portion of $N(t)$ shown in Fig. 1. The created particles are ejected from the interaction zone creation and therefore can no longer block the further pair creation associated with the Pauli-exclusion principle.

The middle part of the probability density oscillates with wavelength λ in Fig. 3(a). This oscillatory structure could be the result of the periodic nature of the creation process where

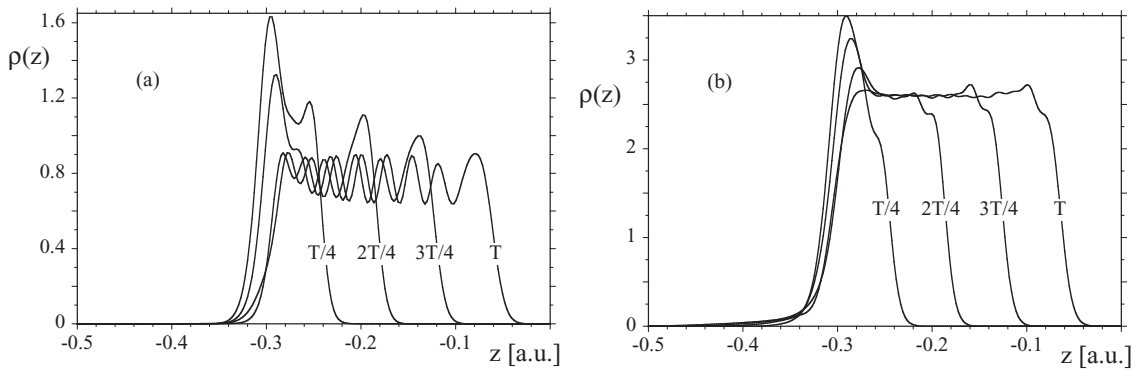

FIG. 3. Snapshots of the probability density $\rho(z,t)$ for $\omega = 1.5\ c^2$ (a) and $2.5c^2$ (b) at times $t = 0.0005$, 0.0010, 0.0015, and 0.0020. Note that the maximum of the electric field is at $z = -0.3$ a.u. [$V_1 = 1.47c^2$, $V_2 = 2.53\ c^2$ $W = 3/c$, $L = 1.2$, $N_z = 512$].

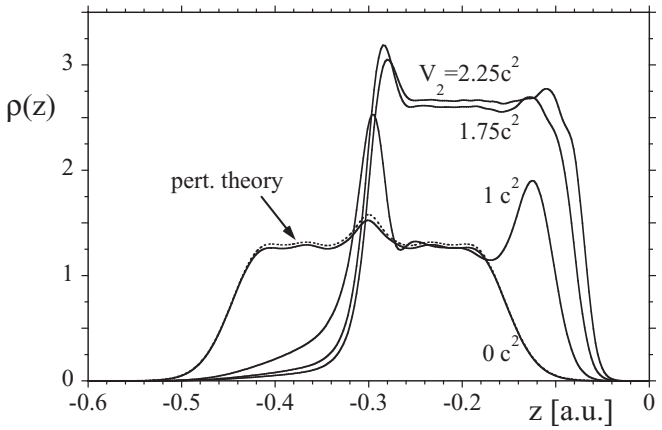

FIG. 4. Final spatial distribution $\rho(z,T)$ for $V_2 = 0c^2, c^2, 1.75c^2, 2.25c^2$ [$V_1 = 1.47c^2$, $W = 3/c$, $\omega = 2.5c^2$].

only during half of the field cycle particles are created due to single-photon transition, which is then followed by tunneling. During the other half cycle the effective field is too small to permit tunneling. The already created particles on the other hand are being forced to the right out of the interaction zone and escape with a uniform speed. More quantitatively, the spatial oscillation wavelength for $\omega = 1.5c^2$ is 0.0271, or close to $3.7/c$. If we use the expression $\lambda = 2\pi\ v_c\ /\omega$ to estimate the wavelength from the frequency ω of the oscillating field and the estimated peak velocity observed from Fig. 3 we get $\lambda \approx 3.8/c$, which is very close to the observed value.

The density shown in Fig. 3(b) corresponds to the larger frequency $\omega = 2.5c^2$, where the pair creation is mostly due to single-photon transitions. As a result, the creation probability is less oscillatory in time and the density of the created particles exhibits less spatial variation for this strength for the static field.

In Fig. 4 we compare the final distribution of created electrons with and without the participation of the time-dependent field V_1, for four different potential heights V_2. Here we choose a frequency $\omega = 2.5c^2$, where the amounts of production for both fields do not differ too much thus making the comparison easier.

As expected, in the limiting case of no static potential ($V_2 = 0$) the distribution is rather symmetric around z_0, reflecting the ejection of an equal amount of electrons into both sides of the oscillating potential. The dashed line represents the prediction by the time-dependent perturbation calculation, which is nearly identical to the exact distribution.

The curve for $V_2 = c^2$ shows that now the electrons are mainly ejected into the positive z direction. It is interesting that the area under the density, which corresponds to the total number of created pairs, amounts to 0.3877. This is slightly less than 0.399 obtained for $V_2 = 0$. It seems that the presence of the static potential inhibits the temporally induced pairs in this case. While the potential-free case permits the electrons to be ejected in both directions, the force due to the static potential may shut off the decay channel and does not allow the electrons to leave (from the left) the interaction zone leading to a blocking of the pair-creation process due to the Pauli-exclusion principle. As we saw in Fig. 2, it depends rather sensitively on the value of ω whether the static field drags the created electrons out of the interaction zone or whether it can reverse the motion of electrons to permit a further inhibition. We will discuss this below.

For larger strengths $V_2 = 1.75c^2$ and $V_2 = 2.25c^2$ this enhancement due to the large force begins to dominate, leading to $N(T) = 0.629$ and 0.653, respectively. The shut off is more apparent at larger still values of V_2 which are not shown here. For $V_2 = 3c^2$, the amount of production is only $N(T) = 0.603$, indicating a decrease.

The additional presence of the static potential introduces three different new mechanisms, one of which suppresses the temporally induced production, whereas the other two enhance it.

The suppression mechanism is based on the fact that due to the tilt of the potential the created electrons can no longer escape in both spatial directions after their creation. In fact, the created electrons that would normally escape to the left are forced to return to the interaction zone where, due to their presence and the associated Pauli blocking, less electrons can be produced. This spatial channel closing (SCC) mechanism should become effective if potential V_2 is strong enough to decelerate electrons and reduce the kinetic energy at birth to zero. In this sense we expect the onset of this SCC mechanism to depend on the details of the temporally induced dynamics such as the frequency ω.

As a second mechanism the downward tilt of the interaction potential could possibly increase the pair production by providing a means to more effectively deplete the interaction zone to the right. It is important to note that this mechanism cannot cancel out the SCC effect. Because it affects only the electrons that were created with velocities pointing to the right while the first mechanism applies to the electrons created with a velocity pointing to the left.

The third mechanism occurs if the strength of the static field is very large (supercritical), such that (even in the absence of temporally induced pairs) the associated force can generate electrons.

The data of Fig. 4 suggest that there might be an optimal value for V_2 for which a maximum amount of pair creation can be achieved. To examine this highly nonmonotonic behavior of the final number of pairs with the strength of the static potential V_2, we graph in Fig. 5 the yield $N(t)$ as a function of the V_2.

The constant graph for small values of V_2 is expected in Fig. 5(a), as the presence of the static field is irrelevant and the creation is entirely due to the time-dependent field V_1 with $\omega = 1.5c^2$. The kinetic energy distribution of the (temporally induced) electrons at the moment of their creation ranges from 0 to $(\omega - 2c^2)$ is centered at around the most likely value of $E_{\rm kin} = (\omega - 2c^2)/2$. The static potential can only affect these particles if $V_2 > (\omega - 2c^2)$, which characterizes the length of the plateau in all graphs shown in Figs. 5(a) and 5(b).

As the static field V_2 is increased it first suppresses the production due to the SCC mechanism discussed above. This leads to the pronounced minimum at $V_2 \approx 0.8c^2$ in each curve in Fig. 5(a) for $V_1 = c^2$ and $1.47c^2$. It is interesting that $N(T)$ decreases again, while in the limit of large V_2 it increases as we show below.

To examine how this decline depends on the frequency ω, we have computed $N(T)$ in Fig. 5(b) again as a function of V_2,

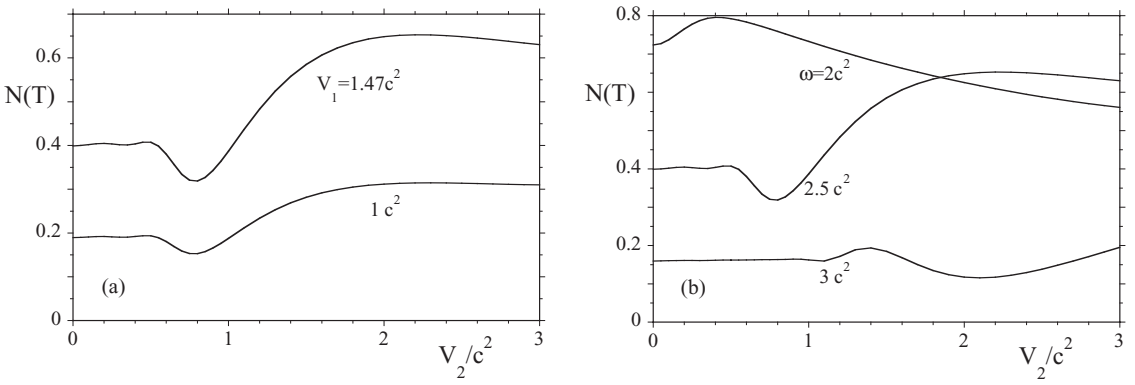

FIG. 5. Total number $N(T)$ as a function of the strength of the static field V_2. (a) $\omega = 2.5c^2$ and two values for V_1. (b) $V_1 = 1.47c^2$ and three values for ω [$W = 3/c$ and $T = 0.002$].

but for three different frequencies $\omega = 2c^2, 2.5c^2$, and $3c^2$ and for the same amplitude of the oscillating field ($V_1 = 1.47c^2$). To better judge the effect of the frequency, we repeat in the middle curve in Fig. 5(b) the top curve of Fig. 5(a). The curve for $\omega = 3c^2$ shows that the location of the minimum is shifted towards larger values of V_2, here it occurs at $V_2 \approx 2.1c^2$, while the overall yield peaks at $N(T) = 0.2$ and is sufficiently less than for $\omega = 2.5c^2$.

As the frequency is decreased to $\omega = 2c^2$, the location of the minimum is shifted to almost $V_2 \approx 0c^2$ and the maximum to $V_2 \approx 0.4c^2$.

If we continue to investigate pair creation for even stronger fields V_2 we find that independent of the value of V_1 the pair creation follows the same law [10,37,38] according to the Schwinger (1D) formula: $V_2 \exp[-2\pi c^3 W/V_2]/(2\pi)$.

V. MOMENTUM SPECTRA SUGGESTING ABOVE THRESHOLD PAIR CREATION

In this section we analyze the pair-creation process with respect to the relevant transitions from the negative to the positive energy states. The momentum resolved electron spectra reveal signatures of various multiphoton induced pair-creation processes.

In Fig. 6 we show the momentum spectrum of the created electrons, defined as $\rho(p,t) \equiv \langle\langle \text{vac}||\hat{b}_p^+(t)\hat{b}_p(t)||\text{vac}\rangle\rangle$, for six different strengths V_1 of the oscillating field and with vanishing static field ($V_2 = 0$). As the total interaction time is about 15 cycles of $2\pi/\omega$, there is a small amount of asymmetry between electrons that are accelerated to positive and negative momentum. Furthermore, while the locations of the peaks seem to be rather independent of the field strength V_1, the shape of the spectrum changes suggesting that a variety of process with different scaling properties each contribute to different portions of the spectrum.

If we convert the locations of the three momentum peaks labeled (A), (B), and (C) to the corresponding energy we find $E_A = 1.255c^2$, $E_B = 2.486c^2$, and $E_C = 3.740c^2$. It is clear that the maximum associated with energy E_A is by far the most dominant one. Its peak height grows nearly quadratically, with a power law $(V_1)^{1.54}$, suggesting a one-photon transition from the initial state with negative energy $E_A - \omega = -E_A$. As the chosen frequency $\omega = 2.5c^2$ is larger than the energy gap, every final electronic state in the energy range $c^2 < E < 1.5c^2$ could become excited via a one-photon transition from the negative energy continuum. However, the coupling matrix element $\langle p|V|n\rangle$ takes its largest value, when the amounts of the corresponding initial and final momenta are identical, making the transition to final energy E_A the most dominant one. We also see a slight change in the slope of the spectrum around $p = 153$ a.u., which corresponds to the highest momentum state (with energy $1.5c^2$) that can be reached via a single-photon transition from the negative energy continuum.

The peak labeled (B) corresponds to a two-photon transition (with an effective power law with exponent 3.86) as indicated by the diagram in Fig. 6. In principle, peak (C) could be the result of an extra photon absorption based on peak (A). While due to the spatial dependence of the external fields this two-photon process is possible in principle, it turns out that the main contributions to this peak are associated with a (comparatively stronger) three-photon transition (with an effective exponent of 5.78). This process is then associated with a consecutive transition from energy from $-E_A - \omega$, to $-E_A$, to E_A, to final energy $E_A + \omega$ ($=3.75c^2$), using $\pm E_A$ as intermediate states. It is very reminiscent of the additional maxima observed in the multiphoton ionization spectra of atoms, called above-threshold ionization and studied

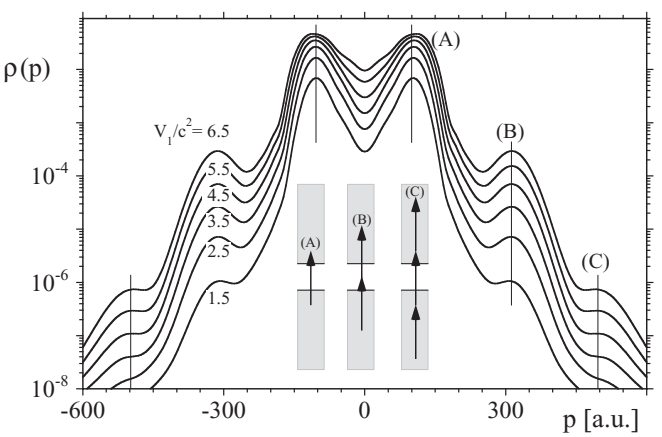

FIG. 6. Momentum density of the pair production for an oscillating field only ($V_2 = 0$) and with six strengths V_1 [$W = 3/c$, $\omega = 2.5c^2$, $T = 0.002$].

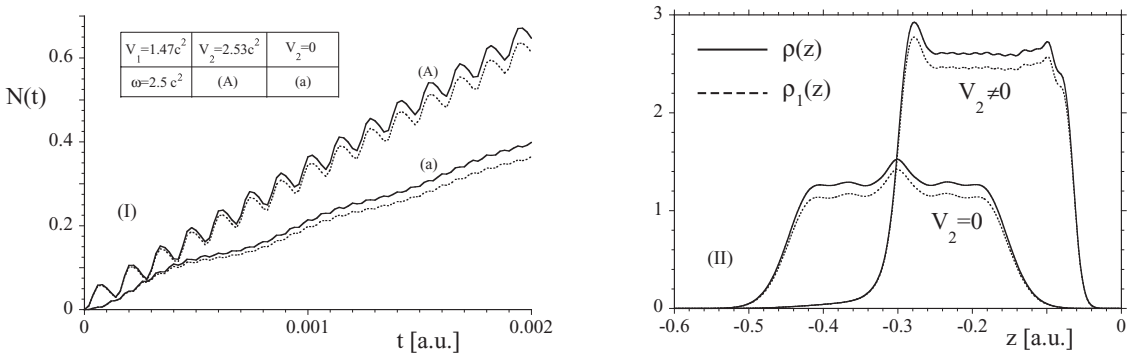

FIG. 7. Comparison of the production for the total number N_∞ (solid) and single pair N_1 (dash). For line (A) $V_1 = 1.47c^2$, $V_2 = 2.53c^2$, for line (a) $V_1 = 1.47c^2$, $V_2 = 0$ [$W = 3/c$, $\omega = 2.5c^2$].

extensively both theoretically and experimentally in the 1980s and 1990s [39]. Using perturbation theory one would expect the height of peak (C) to scale with the sixth power the amplitude V_1, as its strength should be proportional to the square of the product of the coupling matrix elements $\langle -n_A - \omega|V|-n_A\rangle, \langle -p_A|V|-n_A\rangle$, and $\langle -p_C|V|-p_A\rangle$. The observed peak heights confirm this scaling.

It is rather interesting to observe energies close to the location C can also be excited due to two-photon transitions but shifted up in a nonsymmetric way. As a result this process contributes to the background of peak (C). While the absence of any intermediate state at energy zero makes the peak (B) less likely than (C), the lower final continuum energy E_B compared to E_C makes (B) more likely. The data shows that for the whole range of amplitudes V_1 the peak (B) is relatively stronger, suggesting that due to many field induced level shifts, the (bare energy level based) distinction between on- and off-resonant transitions becomes irrelevant for sufficiently strong fields.

One should also point out that peak (B) is unique as it turns out that the nonsymmetric two-photon process can also excite energies close to the position of peak (A) and peak (C) but neither one- nor three-photon process can excite the position where peak (B) is. For this reason the power law for peak (B) is observed for the widest range of amplitude V_1, while the expected power laws with integer exponents only emerges for weak fields for peak (A) and for large fields for peak (C). It appears that stronger field can contribute to the (ponderomotive) shift of the continuum threshold and affect the scaling laws for peak (A). Furthermore, for weaker field this shift prohibits the occurrence of an isolated peak at (C) and the expected power law.

VI. SUMMARY AND DISCUSSION

In this paper we discussed the electron-positron pair-creation process triggered by a combination of a subcritical time-dependent and a supercritical static field. We find that the amount of pair production can be greatly enhanced compared to the yield obtained by the individual fields. The presence of a static field can increase the frequency range of the alternating field where pair creation can occur. The spatially resolved densities show that the static potential plays a crucial part of breaking the spatial symmetry of this system, permitting the rapid escape of particles created by the alternating field from the interaction zone, thus reducing the effect of the Pauli blocking. Furthermore, according to the results of our simulations, in this model the frequency of the alternating field is the most crucial parameter for the process of pair creation, as the created number depends rather strongly on it. We also found the unexpected result that the height of the static potential determines the final yield in a very nonmonotonic way. In fact, one can find amplitudes of the static potential for which the final yield can take maximum as well as minimum values.

In the above results, single as well as multiple electron-positron pairs were created. In order to estimate the importance of the multi-pair-creation processes, we can compute the single-pair creation alone defined as $\int dx \int dy\ |\Phi(x,y,t)|^2$. Here the electron-positron pair wave function can be computed as $\Phi(x,y,t) \equiv \langle\langle \text{vac}||\hat{\Psi}^{(p)}(x,t)\hat{\Psi}_c^{(n)}(y,t)||\text{vac}\rangle\rangle$, where $\hat{\Psi}_c^{(n)}$ is the positronic portion of the field operator.

Figure 7 compares the yields associated with only single pairs with those obtained above which includes the possibility of multiple pairs. We see that for our parameters the total production yields are dominated by single pairs, but the deviation grows with time. The graph in the corner shows the corresponding probability distribution at $t = 0.002$, the two yields deviate of these two numbers lies in not only around the center part, but also in the outside region. Therefore, one can approximate the total production with the amount of just one single pair in this case, especially for short times, when the deviation between the solid and dash line is relatively small.

In all simulations above we have assumed that the spatial extensions of the two associated electric fields W are identical and it would be interesting to examine the dynamics for the case they are different. We also examined (not presented here) the dependence of the total pair creation on the width of second potential W_2. It turned out that the graphs also have maximum and minimum values for different widths of the second potential. The dependency on parameters W_1 and V_2 and the shape of the curves, however, does not change too much either. This is surprising as one does not expect the result to change much for very large values of W_2 where the time-independent field corresponds to spatially constant force field. But our preliminary results show a dependence on W_2. Obviously such a result requires further investigations.

In Sec. III we demonstrated how the usual time-dependent perturbation theory could help us understand the pair creation

in oscillating fields. However, such a theory cannot be applied to the case when an additional static field is present as the energy levels are no longer steady in space and time. We also showed that in this case a simple model in which only two-energy levels are coupled (Appendix B) can describe the complicated dynamics including multiphoton and constant field induced pair creation rather accurately. This model is capable of reproducing all essential features qualitatively in the pair-creation probability. On the other hand, this model has its own limitations as it assumes that the external field is infinitely extended. For example, it cannot describe any spatial distributions of the created particles, which as we have seen in our studies can provide some complementary information about the underlying physical mechanisms. Because the two-level model does not have spatial information it fails to predict the locations of the minima and maxima in Figs. 2 and 5. As we have shown, these depend rather sensitively on the spatial form of the fields. Nevertheless the two-level model can still help us to understand the interplay between the multiphoton processes and the Schwinger tunneling during pair creation. On the other hand, perturbation theory can reproduce the spatial density (as shown in Fig. 4) only in the absence of a static field.

The above-threshold transition and the corresponding structure in the created electron momentum-energy spectrum provide us with another angle to analyze the complicated dynamics. In Sec. V we analyzed one-, two- and three-photon processes and found that at sufficiently high enough intensities ponderomotive energy level shifts will also start to play a role. Such shifts have led to significant modifications in the lower energetic peaks of photoelectron spectra in above-threshold ionization of atoms and molecules by strong laser pulses. As the photoionization mechanisms are not that different as those leading to pair creation, one could expect that these shifts will play a similar role in suppression of the lower energy peaks. In this work we assumed that the detected electrons are outside of the interaction region. When the momentum is measured directly in the interaction zone (or similarly for very short pulses) the energy peaks could experience shifts. The observed increase in the momentum distribution around $p = 0$ may be due to a larger density as predicted by the relativistic energy-momentum relation. Perturbation calculations support such an observation but perturbation theory becomes invalid for larger transition probabilities. We plan to study the interesting low-energy domain in more detail in future work, examining also how the Schwinger tunneling modifies the energy spectrum.

ACKNOWLEDGMENTS

We enjoyed several helpful discussions with Drs. C. Müller, R. Wagner, Y. T. Li, Z. M. Sheng, and J. Zhang. This work has been supported by the NSF and the NSFC (Grant Nos. 11128409 and 11135012). Q.S. and R.G. acknowledge the kind hospitality of their host institutions during their sabbatical leaves.

APPENDIX A: TIME-DEPENDENT PERTURBATION FOR OSCILLATING FIELD

The Hamilton of the system of interest can be separated into two parts, $H = H_0 + H'$. The "unperturbed" Hamiltonian is chosen to be the force-free Hamiltonian for the (two-component) Dirac equation, $H_0 = c\sigma_1 p + \sigma_3 c^2$. The normalized eigenvectors for the Dirac equation $H_0|\Psi\rangle = E|\Psi\rangle$ for positive energy $E_p = \sqrt{(c^4 + c^2p^2)}$ and negative energy $E_n = -\sqrt{(c^4 + c^2n^2)}$ are given by

$$\Psi_+(p,z) = \frac{\begin{bmatrix} \sqrt{E_p + c^2} \\ \mathrm{sgn}(p)\sqrt{E_p - c^2} \end{bmatrix}}{\sqrt{2E_p}} \frac{e^{ipz}}{\sqrt{2\pi}} \quad (\text{for } E_p \geqslant c^2), \tag{A1a}$$

$$\Psi_-(n,z) = \frac{\begin{bmatrix} \mathrm{sgn}(n)\sqrt{-E_n - c^2} \\ \sqrt{-E_n + c^2} \end{bmatrix}}{\sqrt{-2E_n}} \frac{e^{-inz}}{\sqrt{2\pi}} \quad (\text{for } E_n \leqslant -c^2), \tag{A1b}$$

where $\mathrm{sgn}(p)$ denotes the sign of the momenta p and n.

Let us now assume that the perturbation $H' = V(z)\sin(\omega t)$ is suddenly turned on at time $t = 0$. The first-order transition amplitude from the negative state $|\Psi_-(n)\rangle$ to a positive state $|\Psi_+(p)\rangle$ at a time t is given by

$$C^{(1)}_{pn} = \frac{1}{i}\int_0^t \langle\psi_+(p)|H'|\psi_-(n)\rangle e^{i(E_p - E_n)\tau} d\tau = \frac{V_{pn}}{i} f(t), \tag{A2}$$

where $V_{pn} \equiv \langle\Psi_+(p)|V(z)|\Psi_-(n)\rangle$ and

$$f(t) = \int_0^t \sin(\omega\tau) e^{i(E_p - E_n)\tau} d\tau = \frac{1}{2}\left(-\frac{e^{i(E_p - E_n + \omega)t} - 1}{E_p - E_n + \omega} + \frac{e^{i(E_p - E_n - \omega)t} - 1}{E_p - E_n - \omega}\right). \tag{A3}$$

The second term becomes dominant when $E_p - E_n - \omega \approx 0$, thus the first term is negligible and will be omitted, even though keeping the first part does not make the calculation below more difficult.

For the case of the Sauter potential $V(z) = V_0/2[1 + \tanh(z/W)]$, we obtain

$$\begin{aligned} V_{pn} &= \frac{V_0}{2} A_{pn}\left[\int_{-\infty}^{\infty} \tanh\left(\frac{z}{W}\right) e^{-i(p+n)z}\, dz + 2\pi\delta(p+n)\right] \\ &= \frac{V_0}{2} A_{pn}\{-i\pi W/\sinh[\pi W(p+n)/2] + 2\pi\delta(p+n)\}, \end{aligned} \tag{A4}$$

where the inner product for spins A_{pn} is defined as

$$A_{pn} = \frac{\mathrm{sgn}(n)\sqrt{E_p + c^2}\sqrt{-E_n - c^2} + \mathrm{sgn}(p)\sqrt{E_p - c^2}\sqrt{-E_n + c^2}}{4\pi\sqrt{-E_p E_n}}. \tag{A5}$$

The total number of created electrons $N(t)$ and its spatial distribution $\rho(z,t)$ is thus

$$N(t) = \int_{-\infty}^{\infty} dp \int_{-\infty}^{\infty} dn \mid C_{pn}^{(1)} \mid^2, \tag{A6}$$

$$\rho(z,t) = \int_{-\infty}^{\infty} dn \left| \int_{-\infty}^{\infty} dp\ C_{pn}^{(1)}\ \psi_p(z) \right|^2. \tag{A7}$$

Note that the δ function in V_{pn} gives no contribution to the total number and electric density for $A_{pn} = 0$ when $p + n = 0$. To calculate the integrals in the formula of $N(t)$ and $\rho\ (z,t)$, we assume that the system is in a box with length L. Then the momentum states are separated by $\Delta p = 2\pi/L$ and we need a substitution of $\int dp \to (2\pi/L)\sum_p$ and $\int dn \to (2\pi/L)\sum_n$. The result will turn out to be L independent when we set $L \to \infty$.

In the long-time limit, the transition probability is given by

$$P_{pn}(t) = \left|C_{pn}^{(1)}\right|^2 = \frac{|V_{pn}|^2}{4} \frac{\sin^2[(E_p - E_n - \omega)t/2]}{[(E_p - E_n - \omega)t/2]^2} \to \frac{\pi t |V_{pn}|^2}{2} \delta(E_p - E_n - \omega). \tag{A8}$$

Following a similar argument leading to the Fermi Golden Rule, in the "long" time limit, the pair-creation rate is

$$\Gamma = \frac{d}{dt} \int_{-\infty}^{\infty} dp \int_{-\infty}^{\infty} dn\ P_{pn}(t) = \frac{\pi}{2c^2} \int_{-p_m}^{p_m} dp \left| \frac{E_n}{n} \right| |V_{pn}|^2 \delta_{E_n, E_p - \omega}\ \theta(\omega - 2c^2), \tag{A9}$$

where $p_m = \sqrt{[(\omega - c^2)^2 - c^2]}/c$. Here $\theta(\ldots)$ is the Heaviside unit step function. This expression shows that in the long-time limit the pair creation has a sharp turn on at $\omega = 2c^2$ similar to the famous weak field photoelectric effect. The dashed line in Fig. 1 is a result of finite time first-order perturbation calculation.

The time-dependent perturbation may be extended to higher orders as well, corresponding to multiphoton transitions, even though the magnitude due to these orders will be dramatically reduced. The second-order amplitude is

$$C_{pn}^{(2)}(t) = -\frac{1}{4} \sum_k\ V_{pk}\ V_{kn}\ \frac{\exp[i(E_p - E_n - 2\omega_0)t] - 1}{(E_p - E_n - 2\omega_0)(E_k - E_n - \omega_0)} \tag{A10}$$

and the transition probability in the long-time limit is given by

$$P_{pn}^{(2)}(t) = \left|C_{pn}^{(2)}\right|^2 \to \frac{\pi t}{8} \left| \sum_k \frac{V_{pk}\ V_{kn}}{E_p - E_n - \omega} \right|^2 \delta(E_p - E_n - 2\omega). \tag{A11}$$

Similarly, the transition probability in the long-time limit for the third-order perturbation is

$$P_{pn}^{(3)}(t) \to \frac{\pi t}{32} \left| \sum_{k'} \sum_k \frac{V_{pk'}\ V_{k'k}\ V_{kn}}{(E_p - E_n - 2\omega)(E_p - E_n - \omega)} \right|^2 \times \delta(E_p - E_n - 3\omega). \tag{A12}$$

These expressions when summed over index p, n, and divided by t will give the second- and third-order pair-creation rates. As a result, the pair creation is expected to show a sudden increase at $\omega = c^2$ due to two-photon pair creation and another increase at $\omega = 2c^2/3$ for three-photon pair creation. These increases are not easily identifiable for the parameters presented in Fig. 2. For smaller widths of the Sauter field and longer simulation times, however, the thresholds for two- and three-photon pair creation in $N(T)$ can be identified as a function of ω.

APPENDIX B: APPROXIMATE THEORY FOR A SPATIALLY EXTENDED POTENTIAL

Before we derive an approximate description for our system, we first have to change the gauge associated with the external field. The creation of the electron-positron pairs has to be independent of the particular gauge. We obtain identical results by choosing gauge in which the scalar potential $V(z,t)$ is zero. For this we need a transformation from $(V,\ A = 0)$ to $(V' = 0,\ A')$

$$V' = V - \frac{1}{c} \partial_t f(z,t) = 0, \tag{B1a}$$

$$A' = \frac{\partial}{\partial z} f(z,t). \tag{B1b}$$

For our case of a time-dependent and a constant potential given by $V(z,t) = V_1 S(z) T(t) + V_2 S(z)$, the required gauge function can be calculated $f(z,t) = \int_0^t cV(z,t)\, dt = cV_1 S(z) \int_0^t T(\tau)\, d\tau + cV_2 S(z)\, t$. As a result we obtain the new vector potential

$$A' = cV_1 \partial_z S(z) \int_0^t T(\tau)\, d\tau + cV_2 \partial_z S(z)\, t \tag{B2}$$

such that the Dirac equation in this new gauge takes the form

$$i \frac{\partial}{\partial t} \Psi(z,t) = \left[c\sigma_1 (p - A'(z,t)/c) + \sigma_3 c^2\right] \Psi(z,t). \tag{B3}$$

As we will see below, in this particular limit, pair creation can be examined by investigating the solution of a set of ordinary differential equations for a two-level system.

The system discussed in this paper uses a combination of an oscillating potential $V_1(z) = V_1\ \sin(\omega t)\ S(z)$ and a static

potential $V_2(z) = V_2 S(z)$, where the Sauter potential was defined as Sauter potential $S(z) \equiv \{1 + \tanh[(z - z_0)/W]\}/2$. In the limit of $W \to \infty$ we obtain $S(z) = 1/2 + (z - z_0)/(2W) + O(W^{-3})$ and $\partial_z S(z) = 1/(2W) + O(W^{-3})$. In this limit the vector potential in Eq. (B2) takes the easier form $A' = cE_1[\cos(\omega t) - 1] - cE_2 t$, where $E_1 \equiv V_1/(2W)$ and $E_2 \equiv V_2/(2W)$. In such a gauge the states do not need to be modified at $t = 0$ since $f(t = 0) = 0$. Note in such a system where the vector potential is only a function of time, we have momentum conservation [4,12] and the system can be viewed as an infinite set of two-level systems with equal momentum coupling between the positive and negative energy states. To be more specific, the general solution of Dirac equation can be written as a linear combination of a fixed momentum p,

$$\Psi_p(z,t) = C_+(p,t)\Psi_+(p,z) + C_-(-p,t)\Psi_-(-p,z), \quad \text{(B4)}$$

with the initial conditions $C_+(p,t) = 0$ and $C_-(-p,t) = 1$ as a way to calculate $U_{pn}(t)$ starting from the $|n\rangle$ state. If we substitute this into the Dirac equation it leads to a set of equations

$$i\partial \begin{pmatrix} C_+(p,t) \\ C_-(-p,t) \end{pmatrix} \Big/ \partial t = \begin{pmatrix} E_p + A'cp/E_p & A'c^2/E_p \\ A'c^2/E_p & -E_p - A'cp/E_p \end{pmatrix} \times \begin{pmatrix} C_+(p,t) \\ C_-(-p,t) \end{pmatrix}, \quad \text{(B5)}$$

where $E_p = \sqrt{(c^4 + c^2 p^2)}$. This equation can be simplified by using unitary transformations as follows:

$$C_+(p,t) = \tilde{C}_+(p,t) \times \exp\left\{-i \int_0^t [E_p + A'(\tau)cp/E_p]\, d\tau\right\}, \quad \text{(B6a)}$$

$$C_-(-p,t) = \tilde{C}_-(-p,t) \times \exp\left\{i \int_0^t [E_p + A'(\tau)cp/E_p]\, d\tau\right\}. \quad \text{(B6b)}$$

This leads to a coupled set of ordinary differential equations (ODEs):

$$\dot{\tilde{C}}_+(p,t) = -(iA'c^2/E_p)\tilde{C}_-(-p,t) \times \exp\left\{2i \int_0^t [E_p + A'(\tau)cp/E_p]\, d\tau\right\}, \quad \text{(B7a)}$$

$$\dot{\tilde{C}}_-(-p,t) = -(iA'c^2/E_p)\tilde{C}_+(p,t) \times \exp\left\{-2i \int_0^t [E_p + A'(\tau)cp/E_p]\, d\tau\right\}, \quad \text{(B7b)}$$

with initial conditions $\tilde{C}_+(p,t) = 0$ and $\tilde{C}_-(-p,t) = 1$. We have investigated this set of ODEs numerically with the routines provided by the GNU Scientific Library.

To calculate the total number of particle pairs, we have to project the evolved state $|n(t)\rangle$ on positive energy eigenstates in the A-gauge $\Psi_A(p,z) = \exp(-if/c)\Psi_+(p,z)$ to form the matrix elements $U_{pn}(t)$ needed for Eq. (2.6), where $f(z,t) = cE_1\, z\, [\cos(\omega t) - 1] - cE_2 tz$. The total pair-creation yield is given by

$$N(t) = \int_{-\infty}^{\infty} dp' \int_{-\infty}^{\infty} dp \int_{-\infty}^{\infty} dz\ \Psi_+^*(p',z) \times \exp[if(z,t)/c]\ \Psi_p(z,t). \quad \text{(B8)}$$

The two-level model discussed here assumes that the field is infinitely extended, in other words, it cannot provide a total yield but only a number density per unit length. In our numerical simulations we have used a spatially localized Sauter fields with a characteristic width W. In order to make a connection between the approximation and our system, we need to scale the two-level calculation result (first by assuming the peak field value) by the factor of L/W_{eff}. Here L denotes again our numerical box length for a simulation and W_{eff} is the effective length of the Sauter field. We (arbitrarily) define an effective length as $W_{\text{eff}} = \int_{-\infty}^{\infty} dz\ [E(z)/E(0)]^2$, with $E(z) = -dV(z)/dz$, and obtain $W_{\text{eff}} = 4W/3$. For example, for $L = 0.964$ and $W = 5/c$ we obtain a factor $L/W_{\text{eff}} = 19.82$. This scaling factor is used to compare the two-level approximation with our numerical results as displayed in Fig. 2.

[1] F. Sauter, Z. Phys. **69**, 742 (1931); **73**, 547 (1931).
[2] J. Schwinger, Phys. Rev. **82**, 664 (1951).
[3] E. Brezin and C. Itzykson, Phys. Rev. D **2**, 1191 (1970).
[4] V. S. Popov, JETP Lett. **13**, 185 (1971).
[5] V. S. Popov, Sov. Phys. JETP **34**, 709 (1972); JETP Lett. **18**, 255 (1973); V. S. Popov, Sov. J. Nucl. Phys. **19**, 584 (1974).
[6] V. M. Mostepanenko and V. M. Frolov, Sov. J. Nucl. Phys. **19**, 451 (1974).
[7] J. C. R. Bloch, V. A. Mizerny, A. V. Prozorkevich, C. D. Roberts, S. M. Schmidt, S. A. Smolyansky, and D. V. Vinnik, Phys. Rev. D **60**, 116011 (1999).
[8] R. Alkofer, M. B. Hecht, C. D. Roberts, S. M. Schmidt, and D. V. Vinnik, Phys. Rev. Lett. **87**, 193902 (2001).
[9] P. Krekora, K. Cooley, Q. Su, and R. Grobe, Phys. Rev. Lett. **95**, 070403 (2005).
[10] R. Schützhold, H. Gies, and G. Dunne, Phys. Rev. Lett. **101**, 130404 (2008).
[11] T. Cheng, Q. Su, and R. Grobe, Phys. Rev. A **80**, 013410 (2009).
[12] G. R. Mocken, M. Ruf, C. Müller, and C. H. Keitel, Phys. Rev. A **81**, 022122 (2010).
[13] M. Jiang, W. Su, X. Lu, Z. M. Sheng, Y. T. Li, Y. J. Li, J. Zhang, R. Grobe, and Q. Su, Phys. Rev. A **83**, 053402 (2011).
[14] T. Cowan, H. Backe, K. Bethge, H. Bokemeyer, H. Folger, J. S. Greenberg, K. Sakaguchi, D. Schwalm, J. Schweppe, K. E. Stiebing, and P. Vincent, Phys. Rev. Lett. **56**, 444 (1986).

[15] I. Ahmad *et al.*, Phys. Rev. Lett. **78**, 618 (1997).
[16] W. Greiner, B. Müller, and J. Rafelski, *Quantum Electrodynamics of Strong Fields* (Springer, Berlin, 1985).
[17] D. L. Burke, R. C. Field, G. Horton-Smith, J. E. Spencer, D. Walz, S. C. Berridge, W. M. Bugg, K. Shmakov, A. W. Weidemann, C. Bula, K. T. McDonald, E. J. Prebys, C. Bamber, S. J. Boege, T. Koffas, T. Kotseroglou, A. C. Melissinos, D. D. Meyerhofer, D. A. Reis, and W. Ragg, Phys. Rev. Lett. **79**, 1626 (1997).
[18] C. Bamber, S. J. Boege, T. Koffas, T. Kotseroglou, A. C. Melissinos, D. D. Meyerhofer, D. A. Reis, W. Ragg, C. Bula, K. T. McDonald, E. J. Prebys, D. L. Burke, R. C. Field, G. Horton-Smith, J. E. Spencer, D. Walz, S. C. Berridge, W. M. Bugg, K. Shmakov, and A. W. Weidemann, Phys. Rev. D **60**, 092004 (1999).
[19] H. Hu, C. Müller, and C. H. Keitel, Phys. Rev. Lett. **105**, 080401 (2010).
[20] H. R. Reiss, Eur. Phys. J. D **55**, 365 (2009).
[21] H. R. Reiss, J. Math. Phys. (N. Y.) **3**, 59 (1962).
[22] A. D. Bandrauk and H. Shen, J. Phys. A **27**, 7147 (1994).
[23] J. W. Braun, Q. Su, and R. Grobe, Phys. Rev. A **59**, 604 (1999).
[24] G. R. Mocken and C. H. Keitel, Comp. Phys. Commun. **178**, 868 (2008).
[25] M. Ruf, H. Bauke, and C. H. Keitel, J. Comp. Phys. **228**, 9092 (2009).
[26] T. Cheng, Q. Su, and R. Grobe, Cont. Phys. **51**, 315 (2010).
[27] P. Krekora, Q. Su, and R. Grobe, Phys. Rev. Lett. **93**, 043004 (2004).
[28] B. R. Holstein, Am. J. Phys. **66**, 507 (1998).
[29] N. Dombey and A. Calogeracos, Phys. Rep. **315**, 41 (1999).
[30] P. Krekora, Q. Su, and R. Grobe, Phys. Rev. Lett. **92**, 040406 (2004).
[31] C. C. Gerry, Q. Su, and R. Grobe, Phys. Rev. A **74**, 044103 (2006).
[32] A. Di Piazza, E. Lötstedt, A. I. Milstein, and C. H. Keitel, Phys. Rev. Lett. **103**, 170403 (2009).
[33] R. Schützhold, H. Gies, and G. Dunne, Phys. Rev. Lett. **101**, 130404 (2008).
[34] G. V. Dunne, H. Gies, and R. Schützhold, Phys. Rev. D **80**, 111301(R) (2009).
[35] M. Ruf, G. R. Mocken, C. Müller, K. Z. Hatsagortsyan, and C. H. Keitel, Phys. Rev. Lett. **102**, 080402 (2009).
[36] L. Allen and J. H. Eberly, *Optical Resonance and Two-Level Atoms* (Dover, New York, 1975).
[37] B. R. Holstein, Am. J. Phys. **67**, 499 (1999).
[38] P. Krekora, K. Cooley, Q. Su, and R. Grobe, Laser Phys. **15**, 1 (2005).
[39] For review, see, e.g., W. Becker F. Grasbon, R. Kopold, D. B. Milošević, G.G. Paulus, and H. Walther, Adv. At. Mol. Opt. Phys. **48**, 35 (2002).